Spontaneous Raman and Surface-Enhanced Raman Scattering Bioimaging

9

Li Lin and Jian Ye

9.1 Raman Imaging

9.1.1 Principles of Raman Spectroscopy and Raman Imaging

Raman spectroscopy, also named Raman scattering after its discoverer the Indian physicist Sir C. V. Raman, relies on the inelastic scattering of incident photons. Typically, when a radiation of frequency ω_0 is incident on the molecules of a sample, a certain number of scattered photons occur at all directions with varied frequencies (Fig. 9.1). Among them, the majority is the elastic scattered photons called Rayleigh scattering, without any change in frequency; and the inelastic scattered photons with a shifted frequency of $\omega_0 \pm \omega_\nu$ are the Raman scattering. The frequency ω_ν is found to be associated to the transitions between molecular rotational or vibrational levels, resulting in the energy of the incident photons being shifted up or down [1]. The Raman shifts for scattering with an energy loss (with a frequency of $\omega_0 - \omega_\nu$) are referred to as Stokes shift, and the others (with a frequency of $\omega_0 + \omega_\nu$) are as anti-Stokes shift.

The unit for expressing Raman shift (also reported as wavenumber) is the inverse centimeters (cm^{-1}), which is directly related to energy and can be converted to wavelength (λ, nm) by:

$$\text{Raman shift} \left(cm^{-1}\right) = \left(\frac{1}{\lambda_{\text{laser}} \ (nm)} - \frac{1}{\lambda_{\text{signal}} \ (nm)}\right) \times 10^7$$

L. Lin · J. Ye (✉)

School of Biomedical Engineering, Shanghai Jiao Tong University, Shanghai, P. R. China
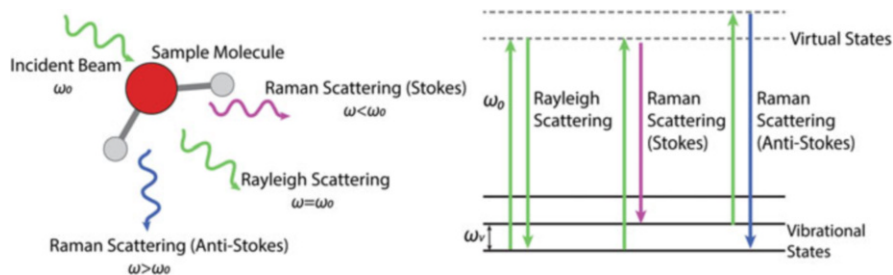
e-mail: yejian78@sjtu.edu.cn

Fig. 9.1 Schematic illustration (left) and energy-level diagram (right) of Rayleigh and Raman scattering process

At present, Raman spectroscopy is widely used in chemistry to provide a molecular fingerprint by which molecules can be identified. The unique Raman shifts in energy offer the structural information of molecules and chemical components, allowing the researchers to detect analytes and obtain their relative concentrations. For the detection of biological samples, Raman spectroscopy provides favorable properties: (1) noninvasive detection capability and high specificity with a fingerprint spectrum, weakly influenced by the temperature or environments; (2) high compatibility with water, which enables the study of biomolecules under the active state in aqueous samples; (3) minimal volume/amount required for the measurement, typically with μL–mL of analytes.

Optical imaging based on Raman spectroscopy is further achieved by collecting and mapping Raman spectra in an area of interest. Either for fundamental studies or in clinical trials, Raman imaging has now been a powerful technique for generating structural images or monitoring minute chemical changes of biological samples such as tumor cells. Basically, Raman imaging can be performed through direct and indirect strategies: the former detects the target directly through the featured Raman spectra of targets; while the latter adopts a Raman label with characteristic peaks to tag and track the targets.

9.1.2 Spontaneous, Surface-Enhanced, and Coherent Anti-Stokes Raman Spectroscopy

If consider within the framework of the energy-level model, spontaneous Raman scattering could be regarded as a process where the perturbation of incident photons makes the molecules transit from the ground state (lowest energy state) to a virtual state, and then molecules spontaneously turn back to the lower state with the emission of new photons (Fig. 9.2). It should be noted that the virtual state does not correspond to any electronic levels, and it cannot be occupied but does allow for transitions between unoccupied real states [2]. This process doesn't literally involve the direct energy absorption. Instead, the role of the incident light is more likely to induce the possibility of the electronic transitions. Nowadays, many types of

Fig. 9.2 Energy-level diagram of CARS process
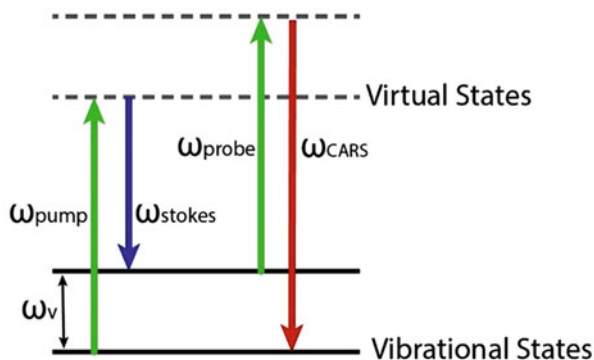
spontaneous Raman spectroscopy techniques have been explored, such as correlative Raman imaging and the resonance Raman spectroscopy. Since Raman scattering highly relies on the chemical information of molecules and is nearly unaffected by the environment, the spontaneous Raman imaging can be used to qualitatively analyze the structure and concentrations of the targets, offering images of high sensitivity and resolution to reveal the details of biological samples.

However, the inherent cross-section (10^{-30} to 10^{-25} cm^2) of Raman scattering is small, compared to that of fluorescence spectroscopy (10^{-17} to 10^{-16} cm^2). This leads to a quiet weak spontaneous Raman signal, and largely limits its application in clinical imaging [3]. The techniques applied to overcome these limitations include the surface-enhanced Raman spectroscopy (SERS) and coherent anti-stokes Raman spectroscopy (CARS).

SERS is a surface-sensitive technique that can greatly amplify the intensity of Raman spectrum of molecules on or near the surface of plasmonic nanostructures. The enhancement factor (EF) can be as high as 10^{14} to 10^{15}, which opens the possibility for single-molecule detection [1, 4]. So far, SERS has been widely used in the field of chemical, biological, or clinical sensing and imaging. It has proven to be an effective and convenient way to amplify the Raman signal of either target or probe molecules. In addition, the capability to analyze each component from a multiplexed mixture on the nanoscale makes SERS superior in performing sensitive and quantitative detection of variant biomolecules, and in obtaining high-quality images of biological structures. The explicit introduction of SERS will be shown in Sect. 9.3.

The coherent nonlinear stimulation can effectively enhance the Raman signal, referred as coherent Raman scattering. One of the developed coherent Raman imaging techniques is based on CARS. As illustrated in the energy-level diagram (Fig. 9.2), the molecule is initially in the ground state, and the pump irradiation (ω_{pump}) excites the molecule to a virtual state. A Stokes beam (ω_{stokes}) is simultaneously present along with the pump, together inducing the energy coupling between the ground state and the vibrational state of the molecule. This coherence can be probed by a probe beam (ω_{probe}), which makes the molecule be excited to a virtual state, and fall back instantaneously to the ground state, leading to the

emission of an anti-stokes photon at the frequency of $\omega_{\text{CARS}} = \omega_{\text{pump}} + \omega_{\text{probe}} - \omega_{\text{stokes}}$. When ω_{probe} equals to ω_{pump} in practical application, the signal $\omega_{\text{CARS}} = 2\omega_{\text{pump}} - \omega_{\text{stokes}}$ is generated with the intensity dependence of a third-order nonlinear optical process [5]. By adjusting ω_{pump} and ω_{stokes} to couple with different molecular vibration energy, the anti-stokes signal can be coherently enhanced and benefit the detection of the corresponding chemical bonds. CARS technique is also label-free and noninvasive, has the capability to show three-dimensional images on molecular components of samples due to its sensitivity to chemical bonds and nonlinear effects. An alternative nonlinear technique is the stimulated Raman spectroscopy (SRS). Together with CARS, they have been studied and shown promises on small molecules tracking and visualization in biological samples. These two techniques are not the main focus in this chapter. Readers are encouraged to find detailed information in the relevant reference [6].

9.1.3   Instrumentation, Data Acquisition, and Spectral Analysis

9.1.3.1 Instrumentation

In a typical setup of Raman microscopic spectrometer, the sample is illuminated with a laser beam, and then the emitted photons from the illuminated spot are collected with a lens and pass through a monochromator. The collected light is dispersed onto a detector with Rayleigh scattering being filtered out using the notch or edge filters. The dispersive spectrographs paired with CCD detectors are commonly used. Among the applied excitation wavelengths for Raman measurements (514, 532, 615, 633, 785, 830 nm, etc.), 785 nm at the first near-infrared window (NIR-I), is the most frequently used in biomedical imaging due to the optimal light penetration depth and the minimization of autofluorescence from biological tissues.

9.1.3.2 Data Acquisition

The most applied method of acquiring spectra for Raman imaging is the pixel-by-pixel point scanning, which requires no technical upgrades on the basic Raman microscopes [7]. Although this strategy has shown enough time resolution to visualize the localization of analytes or nanoparticles (NPs), it leads to a relatively long acquisition time, usually 0.5–20 h for a single-cell imaging (50×50 pixels) if considering that of 0.5–30 s per spectrum.

There have been some techniques developed to accelerate the imaging process in commercial Raman spectrometers. One is the line-scanning method, adopted as the StreamLine™ (Renishaw). Line-scanning acquires spectra from a line of points through a linear laser spot, and can reduce the image acquisition time for the sufficient temporal resolution, rapidly generating high-resolution two-dimensional images of large sample areas in square centimeter scale. It can also prevent laser induced sample damage by illuminating with a line of laser beam, rather than an intense spot. Secondly, Raman imaging can be realized by rapid movement of the laser spot instead of mechanical movement of the sample stage, therefore greatly improving the imaging speed. For example, the Duoscan™ mode (Horiba) uses a

combination of two galvo mirrors that make the laser beam scan across a pattern, either a line for linear profiles or a two-dimensional mapping area. It can be used to generate a "macro laser spot" for a large area with a scanning step size down to 50 nm. Some other techniques, such as multifocus Raman imaging which arranges excitation beams throughout the field of view, or the selective scanning which takes advantages of spatial correlation within samples to reduce the number of spectra required, are also developed in Raman imaging studies to reduce overall acquisition time [7].

9.1.3.3 Spectral Analysis

The Raman spectra for imaging provide high-resolution spatial information of samples, and their raw data also contain spectral information of many interferents. Therefore, it is usually necessary to perform data processing and spectral analysis to deal with the complex dataset for diagnosis and imaging [8].

Spectral preprocessing refers to the treatment before the data are effectively analyzed, aiming to eliminate the interferences of nontarget signals such as autofluorescence background, noise, substrate-generated and other unwanted signals from the sample itself [9]. It could be performed in the following steps: (1) Spectrum smooth. It is applied to a set of Raman spectral data to smooth the high-frequency components without distorting the signal tendency. Savitzky–Golay filter is one of the most popular digital filters applied, which fits successive subsets of adjacent data points with a local polynomial, and can be adjusted by selecting the degrees of polynomials [10]. (2) Background removal, i.e., baseline subtraction. The non-Raman background can be determined and removed while preserving characteristic Raman peaks originating from the sample, by using the polynomial fitting, a wavelet transform, etc. (3) Normalization. Different Raman spectra are often obtained under different experimental conditions and time instruments. The purpose of normalization is to ensure that the Raman spectra of the same materials are as consistent as possible under different test conditions. The common normalizations are based on peak intensity or peak area of a standard material, e.g., a silicon substrate.

After acquiring a group of Raman data with spatial and spectral information (x, y, and Raman shift), a variety of methods can be used to transform them into an image, from direct display of band intensities to more advanced statistical methods [7]. The univariate imaging is a simple way to visualize the locations and relative concentrations of target molecules in the samples, by displaying the intensity of a specific Raman band at each pixel. Advanced multivariate analysis can be further used for complicated samples with multiple components. It exploits the whole spectrum of Raman data rather than relying on a single Raman mode, simultaneously using multiple peaks to display molecular properties and to extract effective information from complex variables. In this case, the minor variations in the spectrum that are unobservable to the naked eyes could convey valuable information. A variety of multivariate analysis methods can be combined and optimized based on the goals of analysis: (1) Data generalization and model construction. For example, principal component analysis (PCA) captures a set of linearly uncorrelated variables

called as principal components to represent the entire dataset, then generates PCA images by plotting the principal components scores at each pixel. (2) Classification. The cluster analysis is adopted to group the sets of similar spectra by assigning colors to each cluster. The average spectrum of each cluster can be analyzed to extract chemical information throughout the sample. (3) Regression to make predictions. The two groups of variables can be correlated and quantified to form a regression model. In this process the coefficients define the relationship between each independent variable and the dependent variable.

9.2 Spontaneous Raman in Biomedical Imaging

9.2.1 Raman Contrast and Label

Spontaneous Raman spectroscopy is capable to provide specific vibrational information of chemical bonds in biomolecules (e.g., lipids, nucleic acids, proteins) as a direct imaging method. The intrinsic bonds with characteristic Raman modes are chosen as label-free chemical contrast in biomedical imaging, such as C–H (2800–3000 cm^{-1}), C=O (1680–1820 cm^{-1}), C–C (stretching mode at 1000–1200 cm^{-1}), and C=C (stretching mode at approximately 1500–1700 cm^{-1}), as shown in Fig. 9.3 [11]. The common biomolecules and their corresponding chemical contrast information can be found in Table 9.1.

Still, spontaneous Raman imaging is hindered by the low sensitivity and weak signals. Some specialized Raman labels have thus been developed to enhance imaging contrast and track molecules. The requirements for the Raman labels are that their bands are easily distinguishable and should not overlap with intrinsic signals of the target molecules. Two excellent candidates are the stable isotope
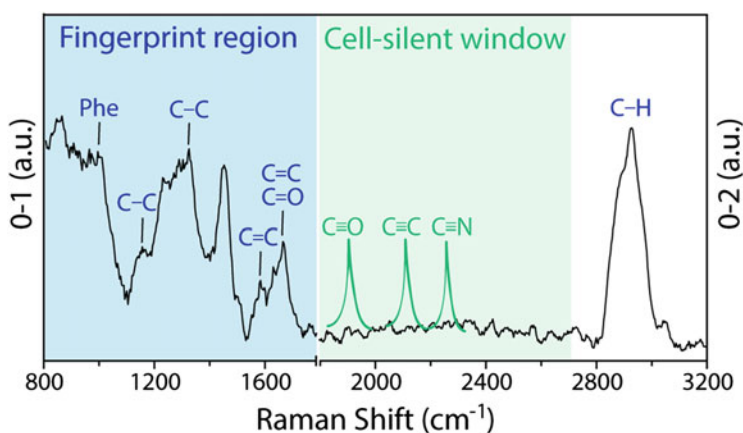

Fig. 9.3 The contrast bands (blue) and label bands (green). The Raman spectrum is measured on an MDA-MB-231 breast cancer cell. The labels exhibit instinct Raman bands in the cell-silent window

Table 9.1 Biomolecules, corresponding contrast and Raman bands, with data adapted from ref. [12, 13]

Biomolecule	Contrast	Raman band (cm^{-1})
Phospholipid	PO_4^{2-}	1090
Lipid	Cholesterol	607, 700, 1440, 1674
	C–C	1065, 1129
	C=C	1660
	C=O	1740
	CH_2 deformation	1300, 1440
	$N(CH_3)_3$	716, 875
Protein	Amide I	1655–1666
	Amide III	1255
	CH_3 deformation	1320, 1450
	Peptide C–C$_\alpha$	898, 935
	Phenylalanine	622, 1004, 1030, 1159, 1208, 1607
	Tyrosine	644, 830, 855, 1175, 1617
	Tryptophan	757, 1159, 1340, 1555, 1617
Nucleic acid	Adenine	727, 1490, 1580
	Cytosine	785
	backbone	830, 1093–1100
	DNA backbone	680, 1490, 1580
	Guanine	667, 757, 780, 1277
	Thymine	

labels and alkyne labels. The stable isotopes (e.g., ^{2}H, ^{13}C, ^{15}N) are used to replace their primordial isotopes (^{1}H, ^{12}C, ^{14}N) [14]. The heavier isotope can lower the vibrational energies of the associated chemical bond, leading to the shifted Raman bands. As the isotope labels can be nondestructively tagged into cellular genomics by cell co-incubation, they enable the direct studies of single-cell metabolism, cell–cell transition and functional properties of microbial communities [14]. Another promising Raman label is the alkyne structure (C≡C), which shows a strong band in the spectral cell-silent window (1800–2800 cm^{-1}). Considering that the 600–1800 cm^{-1} region is generally crowded with intrinsic Raman bands, and the high-frequency C–H stretching mode (2800–3200 cm^{-1}) lacks specificity, the cell-silent window is free from the interference of endogenous cellular background (Fig. 9.3). Also, being small enough not to affect the properties of target molecules, the alkyne structures have been applied to design a kind of alkyne-tagged cell proliferation probes, EdU (5-ethynyl-2′-deoxyuridine), for live cell imaging [15]. Both the stable isotope and alkyl-based Raman label can provide a way with minimal labeling to distinguish the molecules of interest in the spectrum, greatly enhancing the specificity of Raman images.

9.2.2 Spontaneous Raman in Biological Studies

Spontaneous Raman spectroscopy has been shown to measure the slight chemical changes and relative concentrations of components in a single cell, or even at a subcellular level. The visualization of various factors, including the uptake of drugs, bioactive compounds or non-chemical stressors can be obtained [16]. So far, Raman imaging has been be used to study metabolites such as (deoxy)nucleotides, lipids, proteins, amino acids and sugars, playing an important role in fundamental studies of biology, pharmaceutical and medical sciences [11, 17].

9.2.2.1 Nucleic Acid and Proteins Tracking

Nucleic acids and proteins are both essential components in biological cells. The commonly applied imaging method is by staining morphologically preserved fixed cells and tissues. The Raman technique provides an investigation on them in live cells with minimal labels. Sodeoka et al. put forward with the strategies of using alkynes in nucleic acid and proteins visualization [15, 18]. They successfully designed an alkyne-tagged cell proliferation probe, 5-ethynyl-2′-deoxyuridine (EdU), which was readily incorporated into DNA as a mimic of thymidine during DNA replication and can accumulate in nucleus. Thus, the localization of DNA in live cells can be visualized. Alkyne-tagged coenzyme Q (CoQ) analogues were imaged in the same way and their cellular concentrations be semiquantitatively estimated. A simultaneous imaging of the two small molecules, EdU and a CoQ analogue, was also demonstrated. This strategy should be applicable to image a variety of small molecules, such as lipids and drug candidate molecules.

It is noteworthy that in recent years, this method is more adopted by nonlinear Raman imaging techniques, which offers faster image acquisition and greater sensitivity. For example, the alkyne-tagged deoxyribonucleoside ethynyl-deoxyuridine has been used to elucidate DNA synthesis and cell proliferation by SRS [19].

9.2.2.2 Medial Vascular Calcification Imaging

Medial calcification accumulated in the human aorta induces a weakened arterial compliance and is known to comprise a number of diseases. Stevens et al. studied the mechanism of cardiovascular calcification, especially its relationship to atherosclerosis, by using Raman imaging methods [20]. They revealed a biochemical distribution in the aorta by characterizing the Raman spectroscopy of proteins, cholesterol and predominant minerals. Spectral unmixing algorithms were adopted to distinguish between the major biomolecules (apatite, whitlockite, β-carotene, cholesterol ester, triglyceride, elastin, collagen, actin). Raman images of 200 mm × 200 mm with a step size of 0.8 mm × 0.8 mm were acquired using 785-nm laser, 100 mW power and 1 s integration time. For the first time they demonstrated that Raman spectroscopy can be used to quantify the spatial distribution of the mineral species in aortic tissues.

9.2.2.3 Study on Endoplasmic Reticulum (ER) Changes

ER is a cellular compartment where proteins undergo folding and being transported to other parts of a cell or outside cell. The exposure to stressors induces a decreased ER capacity of protein folding and thus an accumulation of unfolded proteins. Majzner et al. have used Raman confocal imaging to monitor biochemical alterations in single endothelial cells under stress stimulated by tunicamycin (Tu) [21]. A 532 nm laser was used with a power of ∼15–20 mW at the sample. Raman imaging was performed on cells with a 0.5 s integration time and a sampling step size of 0.5 µm. They found that Tu accumulation led to the enlarged size of the ER and a decrease of the phospholipid content in the corresponding area. The increased intensity of bands at 790, 1098, 1206, 1342, and 1380 cm^{-1} observed in the ER spectra after Tu treatment indicated that the content of nucleic acids is also bigger. Overall, the application of Raman imaging enabled the studies on the minute chemical information within a single endothelial cell.

9.2.3   Spontaneous Raman in Disease Diagnostics

9.2.3.1 Brain Tumor Biopsy

Limited by the long exposure time, spontaneous Raman imaging is rarely used in vivo or in clinical applications. Still, it can be used on tissues ex vivo for the visualization of tumor sites. J. Popp et al. demonstrate the diagnostic prospects of Raman imaging to probe the cell density and nucleic acid of brain primary tumor metastases [22]. They collected Raman images of human brain tumor tissue sections and analyzed the data using the multivariate vector vertex component analysis (VCA). The results were compared with the gold-standard histopathological assessment, which uses H&E staining on abnormal tissues to show what type of brain lesion (abscess, tumor) is and whether it is malignant or not. A good agreement of Raman imaging results with H&E staining results was reached after spectral demultiplexing. The morphology obtained in lots of Raman images could be interpreted in a similar way as the H&E staining biopsy. Moreover, it was impressive that the spatial resolution was high enough that individual cell nuclei could be resolved in the Raman images. This work demonstrated the prospects of spontaneous Raman imaging as a biopsy tool for direct vision without labeling.

9.2.3.2 Biochemical Study of Heart Tissues

The biochemical study of heart tissues is important to provide information on infarct and related heart disease. Conventional histological examinations such as hematoxylin and eosin staining is capable of elucidating morphological information on fixed tissues, but cannot be applied in vivo. Takamatsu et al. demonstrated a high-speed spontaneous Raman imaging on rat heart tissues with resonance Raman effect of heme proteins [23]. In their findings, the cardiomyocytes and blood vessels in intact hearts can be visualized via cytochromes from oxy- and deoxyhemoglobin, while those in infarct hearts via cytochromes from collagen type-I. By using spectra extracted by PCA, they imaged the intact and infarcted myocardial sections at the

cellular level without further staining. Their work has shown the potential of spontaneous Raman imaging for studying morphological and biochemical changes of heart tissue based on the molecular components, and is prospective toward in vivo monitoring of cardiac microcirculation and fibrosis.

9.3 SERS in Biomedical Imaging

9.3.1 Mechanism and Advantages of SERS

SERS was firstly discovered by Fleischmann et al. in 1974, when they adsorbed pyridine molecules on the surface of roughened silver electrode and obtained the enhanced Raman spectra of pyridine molecules [24]. It was found that the pyridine Raman signal was enhanced by nearly six orders of magnitude. The observed enhancement cannot be explained simply by the increase in the number of molecules, which turned out to be an enhancement effect associated with rough plasmonic surfaces referred as the SERS effect. Its mechanism has been studied throughout decades, with the contributions of EF usually separated into two main categories [1, 2]:

9.3.1.1 Electromagnetic (EM) Enhancement

It is due to an enhanced electric field near the surface of metallic nanostructures, which is affected by their material, size and shape. When metal NPs are irradiated with incident light, the collective oscillations of conduction electrons at the boundary of NPs are excited as localized surface plasmon resonance (LSPR). This process results in a large local field enhancement near NP surfaces, referred to as EM hot spot regions. The Raman signal of molecules located in hot spots can be greatly enhanced, through the coupling of metallic NPs with both the incident field and the re-emitted (scattered) Raman field: the LSPR firstly amplifies the intensity of incident field which excites the Raman scattering of the molecules, thus increasing the signal; then, the Raman scattering signal is further amplified due to the same mechanism, bringing an increase in total EF. The electric field is enhanced as $|E|^2$ at each stage. When both the incident light and the scattering resonate with plasmon frequency, the maximum enhancement can be obtained as the fourth power of the incident field $|E|^4$. EM is thought to be the main contribution to SERS EF, and is nonselective that gives the same enhancement to all types of molecules on the surfaces either through chemisorption or physisorption.

9.3.1.2 Chemical Enhancement (CE)

It is due to the electronic interaction between chemically adsorbed molecules and metallic surfaces. CE can be understood in a way that the interaction induces the formation of intermediates which have a larger scattering cross-section than that of original molecules. The most widely accepted explanation for this is the so-called charge transfer (CT), which can be from the highest occupied molecular orbital (HOMO) of molecules to the Fermi level of metal, and the Fermi level of metal to the

lowest unoccupied molecular orbital (LUMO). Yet researchers have not reached an agreement on the mechanisms and enhancement contributions of CT effect, of which the reported EF was in a wide range of 10 to as high as 10^7 to 10^8 [25]. Also, there are different explanations for the CT effect, including the vibronic coupling model based on the selection rule [26], tunneling or electron transport at metal–molecule–metal interface [27, 28].

9.3.2   Fabrication of SERS Probes

In SERS imaging, the Raman labels with characteristic spectrum are designed to attach to biological tissues or cells through bio-recognition. Then targets can be evaluated by reading the spectra of labels, as an indirect imaging strategy. These Raman labels are named as SERS probes (or SERS tags), which consist of metallic NPs, Raman reporters, protective layers and targeting ligands [29, 30]. In the fabrication process of a typical SERS probe (Fig. 9.4), each step follows certain strategies and principles of design, aiming to improve the intensity, sensitivity, stability, targeting efficiency and binding ability of the SERS probes.

9.3.2.1 Metal NPs

As the core of a SERS probe, the metal NP serves as a substrate to enhance the Raman signal of the molecules adsorbed on the surface. In recent years, plasmonic nanostructures with different sizes and shapes have been intensively studied such as nanospheres, nanorods, nanostars, hollow nanocages and core-shell particles with interior nanogaps. Among them, three types of NPs reported to have ultrahigh EF are: (1) the ones with sharp tips (e.g., nanostars), (2) the assembled NP aggregates with large numbers of hot spots (e.g., NP dimers or trimers), (3) NPs with interior nanogaps as built-in hot spots (e.g., Au core/gap/Au shell NP). Still, Au or Ag nanospheres are the most commonly applied NPs because of their convenient synthetic routes.

9.3.2.2 Raman Reporters

These reporter molecules attached onto the metal NPs endow SERS probes with unique Raman spectra. Generally, the metallic NPs and Raman reporters are the
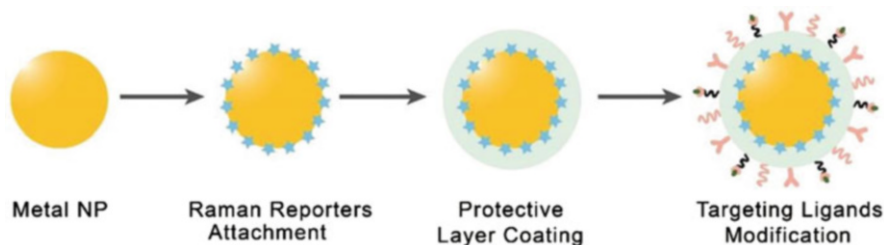

Metal NP   Raman Reporters   Protective   Targeting Ligands
            Attachment   Layer Coating Modification

Fig. 9.4 Fabrication process of a typical SERS probe

basic unit of a SERS probe to provide the strong and characteristic Raman signals, being decisive on the specificity and sensitivity of SERS imaging. There are several strategies to choose suitable Raman reporters [29, 30]: (1) molecules are with a large scattering cross-section for obtaining strong Raman signals, which typically feature aromatic rings or π-conjugated systems; (2) molecules can be easily adsorbed onto metal substrates through physisorption or chemisorption, e.g., molecules with sulf-hydryl groups, amino groups, and carboxyl groups; (3) molecules should have, but not too many, characteristic Raman bands to minimize the band overlap with other molecules in a multiplexing analysis; (4) molecules with an electronic transition band in resonant with the incident laser are beneficial for the surface-enhanced resonant Raman scattering (SERRS) effect, gaining additional 10- to 100-fold enhancement [31].

9.3.2.3 Protective Layer

The compound of metal NP-Raman reporter is the core of a SERS probe, but this simple structure lacks stability and its Raman signal is easily interfered by the surrounding environment. The protective layer is thus adopted to: (1) enhance the stability and biocompatibility of NPs by replacing the original stabilizers or surfactants on their surface; (2) offer the anchoring sites for targeting ligands; (3) protect Raman reporters from directly contacting and being affected by the solution medium. The materials of protective layers can be silica, mesoporous silica, polymers (including polyethylene glycol, polyvinylpyrrolidone, polydiacetylenes), dihydrolipoic acid, *etc*. Nowadays, silica is mostly adopted due to its easy fabrication, and has been applied in commercial Nanoplex™ biotags—a type of silica coated Au NP SERS probes.

9.3.2.4 Targeting Ligands

In the final step of fabrication, the ligands are conjugated to the surface of SERS probes. This step is of critical effects in imaging specificity since the interaction between ligands and targets leads SERS probes to migrate to specific sites. The selection of ligands, including proteins, nucleic acids, aptamers, and small biomolecules, depends on the types of target molecules, e.g., receptors on the tumor cell surface.

The SERS probes facilitate the researches and applications of Raman-based imaging and detections owing to its impressive advantages over conventional optical labels (e.g., organic fluorescent dyes and quantum dots) [32]:

1. High sensitivity down to the single-NP detection level.
2. The narrow bandwidth (usually ~10 cm^{-1}) much smaller than that of fluorescent dyes (~50 nm), which minimizes the peak overlapping for various Raman molecules in the multiplex assays.
3. High photostability under continuous laser irradiation.
4. The selectable excitation wavelength by adjusting the morphology of the SERS substrate and choosing a specific Raman molecule.

9.3.3   SERS Imaging in Biological Studies

9.3.3.1 Cell Imaging

The in vitro cell bioimaging yields information on the cellular biomarkers' expression, intracellular organelles, interactions and dynamics, thus being widely applied and playing a critical role in fundamental biological studies. SERS probes are of intrinsic photostability and multiplexing capability, and the surface coating further brings in high specificity and targeting efficiency, making them ideal optical agents. SERS probes can identify cancer cells via the recognition between specific membrane cancer marker and targeting ligands, such as anti-epidermal growth factor receptor (EGFR) antibodies.

As a nondestructive and sensitive detection technique for chemical components in living cells, SERS cell imaging can be applied for studying the biomarker expression on cell membrane. Additionally, it can be adopted to study and visualize the local chemistry and changes in cell micro environment. The main principle for this type of measurement is to use the target-sensitive Raman reporters. For example, in order to detect the dynamic detection of local pH in living cells, the molecules with pH-dependent spectra are favorable, such as 4-mercaptobenzoic acid (MBA) or 2-aminobenzenethiol (ABT) whose carboxyl or amino groups can be protonated at low pH [32]. Typically, the signal ratios of 1423 cm^{-1} mode (COO- stretching mode) to 1076 cm^{-1} (aromatic ring vibration) of MBA molecules can be applied to sense pH variation. Similarly, to detect the cholesterol in living cells, the Au/Ag NPs modified with 4-mercaptophenylboronic acid (MPBA) on the shell surface was developed [33]. MPBA can react with H_2O_2 and convert into 4-hydroxybenzenethiol (HBT), inducing a change in SERS signal. These NPs can be used to quantify and map the intracellular cholesterol via the produced H_2O_2 in cholesterol oxidation process, proving a reliable SERS mapping analysis of intracellular H_2O_2 and cholesterol at single-cell level.

9.3.3.2 Multiplexing Imaging

The multiplexing imaging has also been intensively studied using SERS probes, which is of multiplexing capability of detecting cancer biomarker on the cell membrane, and the concentration of the biomarkers could be calculated through data processing of individual Raman spectrum, demonstrating the potential for high throughput mapping of cancer cells. For example, researchers have applied the ultrasensitive SERS probes as intracellular imaging agents, which can be embedded with different Raman reporters, and modified with different types of targeting ligands: cell-penetrating peptide, mitochondria-targeting peptide, nucleus-targeting peptide. Their characteristic Raman spectrum can be separated to obtain the location of each type of SERS probes in cells. The multiplexing live-cell imaging is achieved in high-speed (10 ms/pixel) with 200 μW laser power and 785 nm excitation [34]. This work demonstrates promising subcellular organelle targeting and multiplexed capabilities for informative SERS cell imaging, also reveals a great potential for the high throughput SERS imaging of living subjects in the future.

9.3.4 SERS Imaging in Disease Diagnostics

9.3.4.1 Tumor Imaging

SERS has emerged as a powerful tool for in vivo imaging and overcomes several limitations of other imaging methods. The biosafety of SERS probes is expected that no evidence of significant toxicity was observed 2-week after administration in mice [35]. The photostability of SERS probes surpasses the fluorophores. Also, they can be used with adjustable laser excitation and allow multiplexing imaging without strong autofluorescence background interference of tissues.

Starting from one decade ago, researchers have achieved in vivo tumor detection on the mice model. In 2008, Nie et al. using polyethylene glycol coated Au NPs as SERS probes with crystal violet molecules as Raman molecules, which can attach to xenograft tumor models by EGFR biomarkers on human cancer cells [36]. Similar experiments were reported by Kircher et al. using carbon nanotubes as SERS substrate [37]. Following these pioneered works, plenty of progress has been made toward in vivo tumor SERS imaging, mainly to reduce acquisition time by developing brighter SERS probes, improving target specificity, and optimizing Raman system and methodologies [29]. So far, different SERS tags have been developed like Au NPs, nanostars, nanorods, gap-enhanced Raman tags (GERTs) and carbon NPs, with a potential for multiplexing tumor imaging, showing broad research interest in engineering and medicine [29, 38, 39].

Researchers have also begun to integrate SERS with other imaging modalities, such as fluorescence, photoacoustic imaging, PET, CT, and MRI. Gambhir et al. has invented a unique triple modal agent for magnetic resonance imaging, photoacoustic imaging and SERS imaging. This tri-modality agent can help delineate the margins of brain tumors in living mice both preoperatively and intraoperatively, showing the promise for precise brain tumor imaging and resection [40]. Similarly, a type of core-shell Au nanorods embedded with fluorophores of high Raman cross-sections was designed as fluorescence-Raman bimodal nanoprobes by Kircher et al. [41]. Their dual-mode imaging has achieved the visualization of tumor sites on mice models of subcutaneous ovarian cancer or the glioblastoma. The work demonstrates the potential of the integrated fluorescence-Raman technique in cancer imaging.

9.3.4.2 Lymph Node Localization

The sentinel lymph node (SLN) is considered as the first station for metastatic tumors to spread to other parts of the body through the lymphatic system. The presence or absence of cancer cells in SLN could be critical in determining the stage of cancers. As a result, the SLN identification is a key step in the investigation procedure for lymphatic metastasis of tumor sites, in which the optical imaging technique is usually applied. The SERS probes can fulfill the requirement as an SLN imaging agent. In recent years, Ye et al. developed the core-shell structured GERTs [42, 43], which is reported to have strong EF, high photostability, long retention time (24 h) in lymph node, convenient usage (injection 2 h before surgery), and good imaging depth (over 2 mm). They not only allow the high-contrast and deep imaging, but provide the dynamic migration trace of SERS probes into the SLN.

The high-resolution three-dimensional margin of SLN can be visualized through quantitative volumetric Raman imaging data processing. It is also possible to apply a portable Raman spectrometer to locate the SLN, proving a promising potential for convenient preclinical applications.

9.3.4.3 SERS Image-Guided Surgery

Despite major advances in targeted drug and radiation therapies, surgery is still the most effective treatment for localized tumors. Benefited from the development and application of portable Raman scanners and Raman endoscopes, precision cancer surgery guided by intraoperative Raman imaging has been explored in biomedical studies [44]. A SERS probe with high brightness, good targeting capability and specificity can be beneficial for the complete tumor resection surgery of the primary tumor, draining lymph nodes and metastatic sites. Ye et al. developed a type of sensitive core-shell SERS NPs with embedded Raman reporters, showing a detection limit of 20 fM in aqueous solution under laser power density of 10^5 W/cm^2 and 1.86 s integration time [38, 45]. These SERS probes can be applied to identify the tumor margin and locations of micro satellite metastases, as demonstrated in mice for the successful diagnostics of disseminated ovarian cancers, as well as the treatment of the prostate tumors, opening the possibility for more complete tumor resection.

Since SERS probes have large surface areas for functionalization, it is also possible to incorporate other therapy methodologies, including photodynamic therapy, photothermal therapy, and chemotherapeutic delivery, to achieve an image-guided therapy. For example, plasmonic NPs can be served as photothermal agents due to their intrinsic EM enhancement ability. Under continuous irradiation, the SERS probes can have high-enough temperature as the therapeutic agents for image-guided photothermal ablation of tumors [46]. Also, by loading drugs in the surface coating layer of SERS probes, one can perform the Raman-guided chemo-photothermal synergistic therapy [47]. This can be designed for the SERS probes to precisely bind to tumor sites, revealing tumor margin, releasing drugs under the irradiation, killing tumor cells in high temperature, and thus minimizing the side effects on normal tissues. It proves that SERS probes are a robust platform for the intraoperative diagnosis and treatment of tumors.

9.4   Perspective and Conclusions

Raman imaging, including spontaneous Raman and SERS microscopic imaging technique, have been explored to provide the high-resolution noninvasive molecular analysis of biological samples, and shows a breakthrough potential for the diagnoses on human diseases.

Spontaneous Raman imaging is capable to obtain label-free chemical images of samples especially in vitro. Various strategies have been adopted to optimize its performance, such as developing advanced instruments, or enhancing contrast by attaching Raman labels. However, it is still far from clinical application due to the limitations of imaging speed. Huge research opportunities exist in its data acquisition

techniques, spectral processing and analysis methodologies. For example, Raman systems should be updated by reducing either the scanning or data collecting time for high-speed and wide-field imaging. A small-animal Raman imaging system with a speed of 1.5 min for a 5 mm × 5 mm area was reported, showing a tenfold and 240-fold improvement in scan time compared with the Streamline™ (Renishaw) and the normal scan mode, respectively [48].

In contrast, SERS imaging possesses several advantages over spontaneous Raman imaging with reduced time, better photostability, sensitivity, and capability of multiplexing imaging, and has achieved huge progress during the past decade. Nevertheless, the most threatening impediment to its general application is still the imaging speed, particularly compared to that of fluorescence imaging. Its typical exposure time on a single cell is in minutes, which may damage the biological samples and hinder the high-resolution live cell imaging. Efforts have been devoted in two aspects to circumvent this problem. The first is to develop advanced Raman spectrometers, which can also be used for spontaneous Raman imaging. The second is to invent brighter SERS probes. A series of work has been undertaken so far. For example, a type of core-shell probes with the embedded Raman reporters and the petal-like Au shells were reported to have a 10^9 EF and the single-NP detection sensitivity. They allowed the high-resolution cell imaging within 6 s in an area of 50 × 50 pixels, under a 370 μW laser by using the commercial confocal Raman microscopy. In vivo imaging on mice models using the same power and an acquisition time of 0.7 ms per pixel on an area of 3.2 × 2.8 cm^2 was also achieved, which enables high-contrast Raman imaging with a signal-to-background ratio up to ~80 [49].

Like other optical imaging techniques, the tissue penetration in SERS imaging is limited by the absorption and scattering of photons. This hinders the deep tissue imaging on large animals or whole-body scanning on humans. Attempts to circumvent this problem including the development of SERS probes for the second near-infrared window (NIR-II). The NIR-II region of 1000–1700 nm has drawn much attention in bioimaging due to its high improvement in penetration depth and spatial resolution by reducing scattering, absorption, and autofluorescence of tissues. Researches on a direct comparison between NIR-I and NIR-II SERS have demonstrated that the latter provides more favorable optical conditions on biological tissues than the former [50]. It thus would be a great benefit for the studies and applications of SERS imaging with suitable NIR-II probes. Other efforts have been put on the development of multimodal SERS probes, which integrates SERS with other imaging techniques (such as photoacoustic imaging, PET, CT, and MRI) to overcome the limitations of tissue penetration in optical imaging.

Finally, although a variety of fascinating SERS probes have been developed, there are still many obstacles needed to overcome for clinical application, which requires the regulatory approval of the inert NPs based on the knowledge of the pharmacokinetics and toxicity related to metallic, inorganic, and polymeric materials.

References

1. Langer J, Jimenez De Aberasturi D, Aizpurua J, Alvarez-Puebla RA, Auguié B et al (2020) Present and future of surface enhanced Raman scattering. ACS Nano 14:28
2. Le Ru E, Etchegoin P (2008) Principles of surface-enhanced Raman spectroscopy: and related plasmonic effects. Elsevier, Amsterdam
3. Kneipp J, Kneipp H, Kneipp K (2008) SERS—a single-molecule and nanoscale tool for bioanalytics. Chem Soc Rev 37:1052
4. Lane LA, Qian X, Nie S (2015) SERS nanoparticles in medicine: from label-free detection to spectroscopic tagging. Chem Rev 115:10489–10529
5. Zhang Y, Zhen Y, Neumann O, Day JK, Nordlander P et al (2014) Coherent anti-stokes Raman scattering with single-molecule sensitivity using a plasmonic Fano resonance. Nat Commun 5:4424
6. Cheng J, Xie XS (2016) Coherent Raman scattering microscopy. CRC press, Boca Raton, FL
7. Durrant B, Trappett M, Shipp D, Notingher I (2019) Recent developments in spontaneous Raman imaging of living biological cells. Curr Opin Chem Biol 51:138–145
8. Tan Z, Zhang Y, Thackray BD, Ye J (2019) Improvement of surface-enhanced Raman scattering detection and imaging by multivariate curve resolution methods. J Appl Phys 125:173101
9. Byrne HJ, Knief P, Keating ME, Bonnier F (2016) Spectral pre and post processing for infrared and Raman spectroscopy of biological tissues and cells. Chem Soc Rev 45:1865–1878
10. Člupek M, Matějka P, Volka K (2007) Noise reduction in Raman spectra: finite impulse response filtration versus Savitzky-Golay smoothing. J Raman Spectrosc 38:1174–1179
11. Shen Y, Hu F, Min W (2019) Raman imaging of small biomolecules. Annu Rev Biophys 48:347–369
12. Krafft C, Schie IW, Meyer T, Schmitt M, Popp J (2016) Developments in spontaneous and coherent Raman scattering microscopic imaging for biomedical applications. Chem Soc Rev 45:1819–1849
13. Thomas GJ (1999) Raman spectroscopy of protein and nucleic acid assemblies. Annu Rev Biophys Biomol Struct 28:1–27
14. Wang Y, Huang WE, Cui L, Wagner M (2016) Single cell stable isotope probing in microbiology using Raman microspectroscopy. Curr Opin Biotechnol 41:34–42
15. Yamakoshi H, Dodo K, Okada M, Ando J, Palonpon A et al (2011) Imaging of EdU, an alkyne-tagged cell proliferation probe, by Raman microscopy. J Am Chem Soc 133:6102–6105
16. Kaczor A, Marzec KM, Majzner K, Kochan K, Pacia MZ et al (2018) Raman imaging of biomedical samples. In: Confocal Raman microscopy. Springer, New York, NY
17. Gomes Da Costa S, Richter A, Schmidt U, Breuninger S, Hollricher O (2019) Confocal Raman microscopy in life sciences. Morphologie 103:11–16
18. Yamakoshi H, Dodo K, Palonpon A, Ando J, Fujita K et al (2012) Alkyne-tag Raman imaging for visualization of mobile small molecules in live cells. J Am Chem Soc 134:20681–20689
19. Jin Q, Fan X, Chen C, Huang L, Wang J et al (2019) Multicolor Raman beads for multiplexed tumor cell and tissue imaging and in vivo tumor spectral detection. Anal Chem 91:3784–3789
20. You A, Bergholt MS, St-Pierre JP, Kit-Anan W, Pence IJ et al (2017) Raman spectroscopy imaging reveals interplay between atherosclerosis and medial calcification in the human aorta. Sci Adv 3:e1701156
21. Bik E, Mielniczek N, Jarosz M, Denbigh J, Budzynska R et al (2019) Tunicamycin induced endoplasmic reticulum changes in endothelial cells investigatedin vitro by confocal Raman imaging. Analyst 144:6561
22. Krafft C, Belay B, Bergner N, Romeike BF, Reichart R et al (2012) Advances in optical biopsy--correlation of malignancy and cell density of primary brain tumors using Raman microspectroscopic imaging. Analyst 137:5533–5537

23. Ogawa M, Harada Y, Yamaoka Y, Fujita K, Yaku H et al (2009) Label-free biochemical imaging of heart tissue with high-speed spontaneous Raman microscopy. Biochem Biophs Res Commun 382:370–374
24. Fleischmann M, Hendra PJ, McQuillan AJ (1974) Raman spectra of pyridine adsorbed at a silver electrode. Chem Phys Lett 26:163–166
25. Park W, Kim ZH (2010) Charge transfer enhancement in the SERS of a single molecule. Nano Lett 10:4040–4048
26. Lombardi JR, Birke RL (2009) A unified view of surface-enhanced Raman scattering. Acc Chem Res 42:734–742
27. Lin L, Zapata M, Xiong M, Liu Z, Wang S et al (2015) Nanooptics of plasmonic nanomatryoshkas: shrinking the size of a core–shell junction to subnanometer. Nano Lett 15:6419–6428
28. Lin L, Zhang Q, Li X, Qiu M, Jiang X et al (2018) Electron transport across plasmonic molecular nanogaps interrogated with surface-enhanced Raman scattering. ACS Nano 12:6492–6503
29. Jiang C, Wang Y, Song W, Lu L (2019) Delineating the tumor margin with intraoperative surface-enhanced Raman spectroscopy. Anal Bioanal Chem 411:3993–4006
30. Wang Z, Zong S, Wu L, Zhu D, Cui Y (2017) SERS-activated platforms for immunoassay: probes, encoding methods, and applications. Chem Rev 117:7910–7963
31. McNay G, Eustace D, Smith WE, Faulds K, Graham D (2011) Surface-enhanced Raman scattering (SERS) and surface-enhanced resonance Raman scattering (SERRS): a review of applications. Appl Spectrosc 65:825–837
32. Wang Y, Yan B, Chen L (2013) SERS tags: novel optical nanoprobes for bioanalysis. Chem Rev 113:1391–1428
33. Jiang X, Tan Z, Lin L, He J, He C et al (2018) Surface-enhanced Raman nanoprobes with embedded standards for quantitative cholesterol detection. Small Methods 2:1800182
34. Kang JW, So PTC, Dasari RR, Lim D (2015) High resolution live cell Raman imaging using subcellular organelle-targeting SERS-sensitive gold nanoparticles with highly narrow intra-nanogap. Nano Lett 15:1766–1772
35. Thakor AS, Luong R, Paulmurugan R, Lin FI, Kempen P et al (2011) The fate and toxicity of Raman-active silica-gold nanoparticles in mice. Sci Transl Med 3:33r–79r
36. Qian X, Peng X, Ansari DO, Yin-Goen Q, Chen GZ et al (2008) In vivo tumor targeting and spectroscopic detection with surface-enhanced Raman nanoparticle tags. Nat Biotechnol 26:83–90
37. Zavaleta C, de la Zerda A, Liu Z, Keren S, Cheng Z et al (2008) Noninvasive Raman spectroscopy in living mice for evaluation of tumor targeting with carbon nanotubes. Nano Lett 8:2800–2805
38. Zhang Y, Liu Z, Thackray BD, Bao Z, Yin X et al (2018) Intraoperative Raman-guided chemo-photothermal synergistic therapy of Aadvanced disseminated ovarian cancers. Small 14:1801022
39. Davis RM, Kiss B, Trivedi DR, Metzner TJ, Liao JC et al (2018) Surface-enhanced Raman scattering nanoparticles for multiplexed imaging of bladder cancer tissue permeability and molecular phenotype. ACS Nano 12:9669–9679
40. Kircher MF, de la Zerda A, Jokerst JV, Zavaleta CL, Kempen PJ et al (2012) A brain tumor molecular imaging strategy using a new triple-modality MRI-photoacoustic-Raman nanoparticle. Nat Med 18:829–834
41. Pal S, Ray A, Andreou C, Zhou Y, Rakshit T et al (2019) DNA-enabled rational design of fluorescence-Raman bimodal nanoprobes for cancer imaging and therapy. Nat Commun 10:1926
42. Bao Z, Zhang Y, Tan Z, Yin X, Di W et al (2018) Gap-enhanced Raman tags for high-contrast sentinel lymph node imaging. Biomaterials 163:105–115

43. Zhang Y, Qiu Y, Lin L, Gu H, Xiao Z et al (2017) Ultraphotostable mesoporous silica-coated gap-enhanced Raman tags (GERTs) for high-speed bioimaging. ACS Appl Mater Interfaces 9:3995–4005
44. Karabeber H, Huang R, Iacono P, Samii JM, Pitter K et al (2014) Guiding brain tumor resection using surface-enhanced Raman scattering nanoparticles and a hand-held Raman scanner. ACS Nano 8:9755–9766
45. Qiu Y, Zhang Y, Li M, Chen G, Fan C et al (2018) Intraoperative detection and eradication of residual microtumors with gap-enhanced Raman tags. ACS Nano 12:7974–7985
46. Jin X, Khlebtsov BN, Khanadeev VA, Khlebtsov NG, Ye J (2017) Rational design of ultra-bright SERS probes with embedded reporters for bioimaging and photothermal therapy. ACS Appl Mater Interfaces 9:30387–30397
47. Gandra N, Portz C, Singamaneni S (2014) Multifunctional plasmonic nanorattles for spectrum-guided locoregional therapy. Adv Mater 26:424–429
48. Bohndiek SE, Wagadarikar A, Zavaleta CL, Van de Sompel D, Garai E et al (2013) A small animal Raman instrument for rapid, wide-area, spectroscopic imaging. Proc Natl Acad Sci 110:12408–12413
49. Zhang Y, Gu Y, He J, Thackray BD, Ye J (2019) Ultrabright gap-enhanced Raman tags for high-speed bioimaging. Nat Commun 10:1–12
50. Lane LA, Xue R, Nie S (2018) Emergence of two near-infrared windows for in vivo and intraoperative SERS. Curr Opin Chem Biol 45:95–103